Chapter 20
Finite Element Modelling and Experimental Verification of Dissimilar Joining Between Inconel 718 and SS 316L by Micro-plasma Arc Welding

Ajit Kumar Sahu and **Swarup Bag**

Abstract In the present research work, an attempt is made to successfully weld Inconel 718, a nickel-based superalloy with SS 316L, an austenitic stainless steel in autogenous mode by using constant current micro-plasma welding process. A finite element method (FEM)-based, three-dimensional (3D) thermal model is developed for butt welding configuration between the selected bimetallic combinations by using a double-ellipsoidal volumetric heat source model. A good consistency is found between the numerically obtained and experimentally obtained weld bead measurements. The numerical model is further used to extract peak temperatures, time–temperature profiles along with average cooling rates of the welding processes. Obtained cooling rates are correlated with the weld micro-structures and mechanical properties. Micro-structural study by SEM analysis has shown coarse columnar dendritic structure in the weld interior for the higher heat input welding case, whereas lower heat input during welding leads to fine weld micro-structure due to high cooling rate. An improvement in the tensile strength and hardness value is observed with increase in weld cooling rate and low heat input during the joining process.

Keywords Inconel 718 · Finite element modelling · Dissimilar welding · Cooling rate · Micro-structure

A. K. Sahu (✉) · S. Bag
Department of Mechanical Engineering, Indian Institute of Technology Guwahati,
Guwahati 781039, Assam, India
e-mail: ajit.sahu@iitg.ac.in

S. Bag
e-mail: swarupbag@iitg.ac.in

20.1   Introduction

Welding of dissimilar materials is always a challenging task due to the differences in material composition and physical properties which need several trials to optimize successful welding parameters. Dissimilar material welding has been in demand for various industries to reduce material cost and to improve flexibility in design. It not only satisfies the service condition but also reduces component cost by reducing the amount of high-cost materials in a component [1]. Inconel 718 is a nickel–chromium-based precipitation hardened superalloy which is strengthened mostly by γ'' (Ni_3Nb) precipitates [2]. Excellent corrosion and oxidation resistance along with extensive mechanical properties at elevated temperature makes Inconel 718 suitable for various critical condition applications. Higher resistance to strain age cracking during the welding makes it one of the most successful high temperatures nickel–chromium alloy ever designed. It is widely used to make hot section components of aero engine, liquid rocket cryogenic engines, and gas turbines blades. It is also widely used in chemical industries, process industries, and nuclear reactors in various severe working conditions [3]. Similarly, austenitic steels are widely used in petrochemical, aerospace, and power generating sector in the form of plates, coils, sheets, bars, and tubing. AISI 316L contains lower amount of carbon which makes this austenitic steel immune to the sensitization at elevated temperatures [4]. AISI 316L exhibits higher creep and tensile strength as compared to other nickel–chromium austenitic steels over a wide temperature range. It also possesses excellent toughness even at the cryogenic temperature which makes it distinct from other chromium–nickel austenitic stainless steels.

The aforesaid features of Inconel 718 and AISI 316L make them suitable to use in the form of bimetallic joint for various engineering applications to make various components in aerospace engine and gas turbine engine. This bimetallic combination is used by ALSTOM Power Sweden for making compressor rotor where high pressure compressor stages are made by Inconel 718 and low pressure stages are made of austenitic based stainless steel [5]. Fusion welding is one of the most preferred joining techniques for this bimetallic combination to establish a good metallurgical bond between the mating surfaces. Although fusion welding of Inconel 718 is not utterly free from welding defects, it can be minimized by taking required precautions during welding process. Defects like solidification cracking and micro-fissuring in the fusion zone (FZ) and heat affected zone (HAZ) are major problem associated with the Inconel 718 and AISI 316L [6]. The generation of intermetallic Laves phase by segregation of niobium (Nb) in the interdendritic region during weld metal solidification is the main cause of above welding defects in Inconel 718 [7], whereas formation of 3–9% of δ ferrite reduces tendency of hot cracking, but higher percentage of ferrite content reduces creep life along with corrosion resistance of the AISI 316L joint [8]. A higher weld cooling rate has resulted in minimization of these defects which can be achieved by using a heat source of higher power density [9]. Thavamani et al. [10] have used gas tungsten arc welding (GTAW) process for welding Inconel 718 at three different heat input

of 530, 670 and 800 J/mm and reported the size of dendrites and crack sensitivity of the weld increasing with increase in heat input. Lower value of heat input improves the weld cooling rate, whereas higher value slows down the weld cooling rate which leads to segregation of various useful alloying element into the interdendritic regions, leading to deterioration of mechanical properties of the welded component. Bansal et al. [11] have used microwave welding to join Inconel 718 and AISI316L with Inconel 718 powder as interfacing layer between the two surfaces and reported good joint strength for the bimetallic welded joint. Ramkumar et al. [12] have used multi-pass GTAW process to weld this bimetallic combination of material and reported superior mechanical properties for the joint as compared to the AISI 316L base material. Ramkumar et al. [13] inspected the dissimilar welding of Inconel 718 and SS 316L with the help of constant and pulsed current mode GTAW process. They found weld prepared by pulsed current mode has superior tensile, hardness and toughness properties as compared to constant current mode weld which is mainly due to the control of Laves phase formation due to higher cooling rate, obtained during pulsed current mode of welding. Kumar et al. [4] also employed CCGTAW and PCGTAW to weld Inconel 625 and AISI 316L and stated presence of various secondary phases in the HAZ are minimal for PCGTAW condition. From the above literature review, it can be concluded that the scope and application of joining this bimetallic combination are wider and required through investigation in terms of joint performance at ambient temperature. The selection of proper welding techniques and process condition is an important aspect of welding dissimilar materials. By using advanced welding techniques, full penetration can be achieved comparatively at a lower heat input; as a result, the weld cooing rate can be enhanced and formation of various deleterious secondary phases can be constricted [14]. From the open literature, it was evident most of the reported work were limited to GTAW process for joining this bimetallic combination. Hence, in the present study, micro-plasma arc welding technique which has higher power intensity among all the arc welding processes is used to join this bimetallic combination [15]. μ-PAW also possesses good arc stability even at very low range of current as compared to GTAW which makes this process more suitable for joining thin sheets. The present study is mainly focused on weldability, mechanical and metallurgical analysis of these bimetallic joints obtained at different condition of continuous current μ-PAW process. Another objective of the present study is to correlate the effect of heat input/cooling rate on fusion zone micro-structure and Laves phase formation by different welding condition.

Direct experimental investigations during welding are extremely expensive and often impossible because of the complexity of the process and presence of high temperature arc. Hence, a three-dimensional finite element (FE)-based numerical model was developed using ABAQUS to obtain the temperature isotherm in the fusion zone along with time–temperature history of μ-PAW welding process. The conductive heat transfer-based numerical modelling is done by using a moving double-ellipsoidal heat source that is accountable for complex physical phenomena like conduction, convection along with radiation heat transfer from the joining surfaces to the ambient. The double-ellipsoidal heat source is used in the current

study due to its unique capability to incorporate steep gradient of temperature in the front of heat source and a gentle gradient in the trailing edge of weld pool [16]. Temperature-based physical properties of the materials were considered in the model. Thereafter, the time–temperature profile of the fusion zone from the numerical model is accounted for estimation of the cooling rate. The influence of weld cooling rate/solidification rate on weld micro-structure and corresponding outcome on mechanical properties are reported in the present study.

20.2   Experimental Procedure

As received Inconel 718 and AISI 316L stainless steel sheets of thickness 0.7 mm were sheared into 100 × 60 mm coupons with welding direction normal to the rolling direction, the chemical composition of the base materials were analysed by energy dispersive X-ray (EDX) technique and results are shown in Fig. 20.1. Based on EDX analysis, the resulted composition (wt%) of Inconel 718 and AISI 316L are given in Table 20.1.

The welding surfaces were cleaned with acetone prior to the welding process for removing oxides and other foreign impurities. Sheets were clamped in a restrain fixture made up of copper to achieve high cooling rate. The welding torch of micro-plasma set-up is kept fixed and the workpiece is allowed to move at a constant velocity. Commercially available argon gas (99% pure) is used as plasma gas as well as used as a shielding gas for the protection of weld pool. Butt configuration weld joints were prepared by constant current (CC) mode using micro-plasma arc welding set-up with a DC current range of 0.05–50 A. The plasma gas and shielding gas flow rate are maintained at 0.5 and 5 L/min, respectively, with a nozzle standoff distance of 2 mm. The other welding parameters employed for making defect free welds are depicted in Table 20.2 which is obtained by a wide range of welding trials.
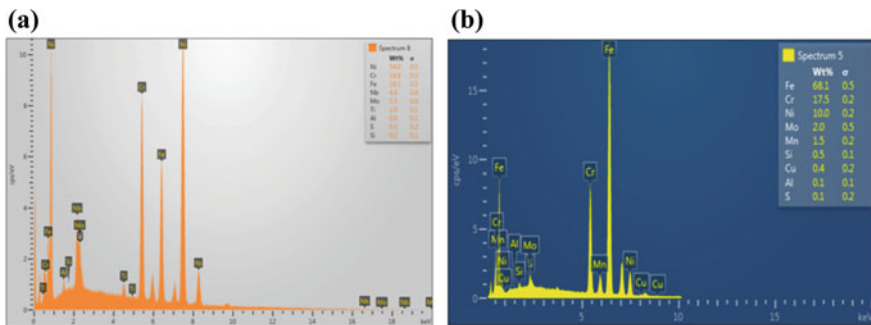

Fig. 20.1 EDX elemental analysis of **a** Inconel 718 and **b** AISI 316L base material

Table 20.1 Chemical composition (wt%) of Inconel 718 and AISI 316L

Elements	Ni	Cr	Nb	Mo	Ti	Al	Si	S	Fe
Inconel 718	54.0	18.6	4.8	2.5	1.0	0.6	0.2	0.2	Bal.
Elements	Ni	Cr	Mo	Mn	Si	Cu	Al	S	Fe
AISI 316L	10.0	17.5	2.0	1.5	0.5	0.4	0.1	0.1	Bal.

Table 20.2 Process parameters for μ-PAW of Inconel 718 and SS 316L weldments

Sample	Current (A)	Voltage (V)	Welding speed (mm/s)	Heat input (J/mm)
S1	14	24	3.4	99
S2	15	24	3.2	112

The welded samples were sheared normal to the welding direction and polished for macro-structural analysis. Then, the mirror polished samples were etched in a mixture of HCl, HF and CH_3COOH in the ratio of 1.5:1:1, respectively, for the micro-structural analysis. The micro-structural analyses were done by the help of optical microscope and scanning electron microscope. Vickers's micro-hardness measurements were done across the weld bead for each specimen to analyse the hardness behaviour. Tensile test of the welded specimens and base materials are conducted at room temperature to analyse the yield strength, ultimate tensile strength and percentage elongation. For each condition, two sub-size transverse specimens were prepared according to ASTM E8 M standard with a gauge length of 25 mm. The tests were conducted by a computer controlled servo-hydraulic universal tensile testing machine with a cross-head speed of 1 mm/min.

20.3   Numerical Model

Experimental investigations have certain limitations due the involvement of high temperature heat source during the welding process. Hence, a finite element-based conduction heat transfer model is developed for the micro-plasma arc welding process to obtain temperature distribution of the entire weldment. The moving heat source is incorporated in the model by using a DFLUX subroutine with the numerical model. To approximate the influence of convective transport of heat in weld pool, a Gaussian distributed double-ellipsoidal volumetric heat source is used to distribute the heat flux into the joining surfaces. Temperature-based thermo-physical properties for SS 316L and Inconel 718 were considered in the present analysis [17, 18]. For simplification, following assumptions were considered in the model: Top surface of the fusion zone is assumed as flat and neglecting the effect of plasma arc and shielding gas. The initial temperature of workpiece was taken as uniform ambient temperature (T_0) of 300 K. The latent heat of melting and

cooling is incorporated, whereas material evaporation from the fusion zone is neglected. The surface of the base plates which is exposed to heat flux and other surfaces is subjected to heat losses due to convection and radiation. The surfaces which are directly exposed to air were assigned a convective heat transfer coefficient (h) of 35 W/m^2 K [16]. However, surfaces which are in direct contact with the copper fixture and backing plate, which have high thermal conductivity, are assigned with a high heat transfer coefficient of 1000 W/m^2 K [19]. The fundamental governing equation of heat transfer or conservation of energy in 3D Cartesian coordinate is expressed as

$$\rho C \left(\frac{\partial T}{\partial t} - v \frac{\partial T}{\partial x} \right) = \frac{\partial}{\partial x} \left(k \frac{\partial T}{\partial x} \right) + \frac{\partial}{\partial y} \left(k \frac{\partial T}{\partial y} \right) + \frac{\partial}{\partial z} \left(k \frac{\partial T}{\partial z} \right) + \dot{q} \qquad (20.1)$$

where (x, y, z) is the coordinate system associated with the moving heat source. ρ, k and C refer to density, thermal conductivity and specific heat of the base material, respectively. T and t represents temperature and time variable, respectively. $\dot{q}$ is the internal heat generation per unit time and per unit volume and 'v' is considered as the velocity of the plasma arc in welding direction (x-axis) or moving coordinate axis. The meshing arrangement of base plate is shown in Fig. 20.2. Very fine meshing is provided in the fusion zone area to capture thermal history precisely as it is exposed to a very concentric heat source where the temperature gradient becomes steep. While coarser meshing was generated in the area far from the heat flux to reduce computational cost, Continuum solid eight nodded brick elements (DC3D8 type) were selected in the thermal analysis for diffusive heat transfer.

The double-ellipsoidal parameters like width (b) and depth (c) of the double-ellipsoidal heat source were directly taken from the experimental results. The length of front (c_f) and rear (c_r) quadrant were estimated as a function of velocity [20]. In dissimilar welding, the fusion zone becomes a mixture of both base materials which will produce various intermetallic compounds during the
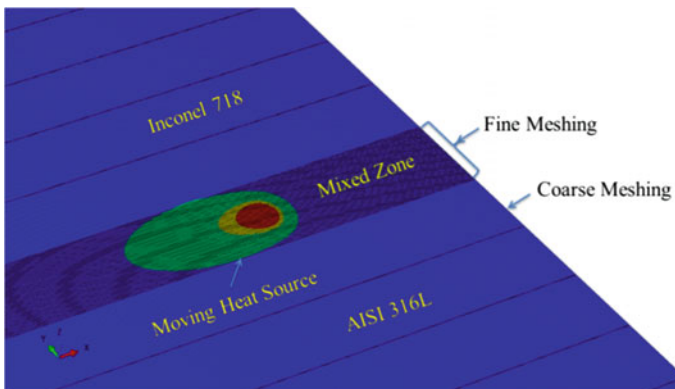

Fig. 20.2 Finite element meshing of solution domain

solidification and will have an impact the joint efficiency. Therefore, to correlate the weld cooling rate with intermetallic phase formation precisely, the temperature dependent thermo-physical properties of fusion zone were considered as the average of both base materials which is named as mixed zone as shown in Fig. 20.2.

20.4   Results and Discussion

20.4.1   *Temperature Field Characteristics*

Temperature distribution corresponding to S1 welding condition along with the moving heat source is shown in Fig. 20.3. A peak temperature of 2169 K is achieved at the weld centre line. The fusion zone (FZ) is defined by 1730 K which is the liquidus temperature of AISI 316L, i.e. maximum between the base materials [1]. And the heat affected zone (HAZ) was defined below 1547 K which is the solidus temperature of Inconel 718, i.e. minimum between the base materials [21]. The region between these two isotherm contours is considered as mushy zone where liquid and solid phase coexists together.

The comparison between simulated and experimentally estimated weld macrographs in transverse cross section for both welding conditions is shown in Fig. 20.4, where FZ, mushy zone, and HAZ are well defined. The shape and size of the numerically simulated outcomes were found to be in good agreement with the experimentally obtained weld macrographs. With increase in welding heat input per unit length, the size of weld bead increases and the fusion zone becomes wider. The weld cross section of S2 welding condition is little bit of straight type as compared
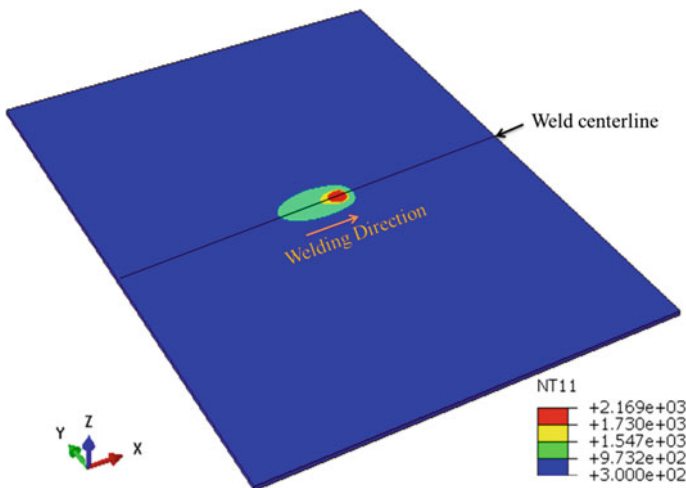

Fig. 20.3 Temperature distribution for S1 welding condition
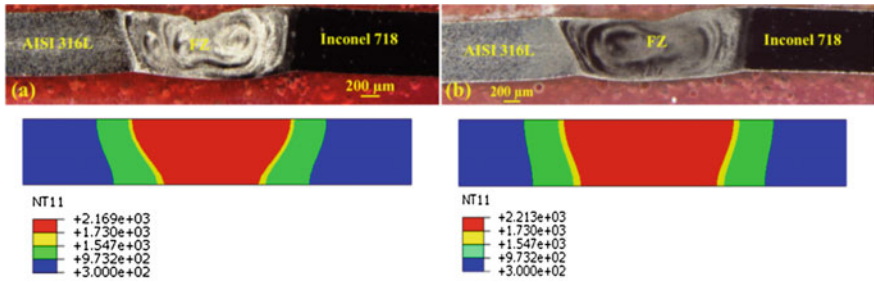
Fig. 20.4 Comparison of weld macrograph for **a** S1 and **b** S2 welding condition

to S1 welding condition which is due to higher heat input during welding process. The maximum error found to be 6% in the weld bead width comparison at the cap and root between experimentally and numerically measured value (Table 20.3).

Figure 20.5 shows the time–temperature profiles of S1 and S2 welding condition at weld centre along with the average weld cooling rate. The temperature rises rapidly as the heat source approaches and drops steadily to ambient temperature when the heat source passes away from the node. The quality of weld is greatly dependent on heat input per unit length during the welding process, peak

Table 20.3 Weld bead dimensions at different location

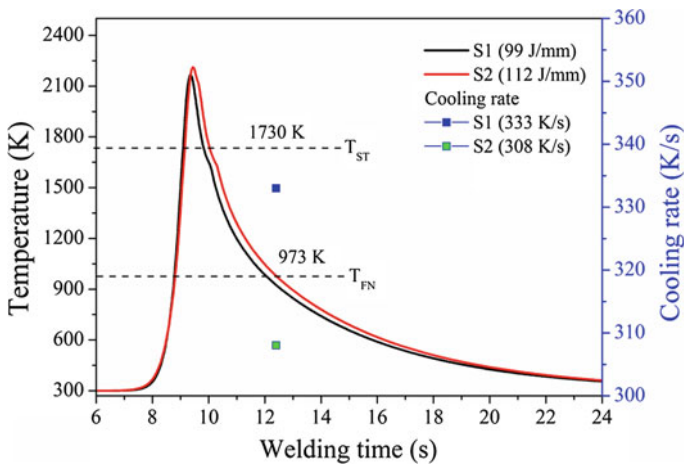| Location	S1		S2	
	Experimental	Numerical	Experimental	Numerical
Weld cap (mm)	2.46	2.38	2.6	2.44
Weld root (mm)	1.91	1.8	1.96	1.94

Fig. 20.5 Time–temperature profile and average cooling rate of S1 and S2 welding conditions

temperature, and cooling rate. The peak temperature of S1 and S2 welding conditions were found to be 2169 and 2213 K, respectively. Higher peak temperature for S2 welding condition is attributed to the higher heat input during welding process. The average weld cooling rate was calculated by taking the slope of time–temperature curve between transformation start (T_{ST}) and finish temperature (T_{FN}). Higher liquidus temperature among Inconel 718 and SS 316L was considered as T_{ST} as below this temperature phase transformation initiated. Minimum value of solid phase transformation end temperature among the bimetallic is taken as T_{FN} as below this temperature phase transformation does not occurs. The calculated average cooling rate for S1 and S2 welding condition were 333 and 308 K/s. When the weld peak temperature increases, weld pool lasts for longer period of time resulted in lower average cooling rate.

20.4.2 Effect of Cooling Rate on Weld Micro-structure and Mechanical Properties

Formation of various intermetallic phases during weld cooling period is the major challenge of fusion welding process. Segregation of Mo and Nb in the interdendritic region leads to formation of deleterious Laves phases in Inconel 718 which promotes liquation cracks and micro-fissuring in the FZ and HAZ [14]. In AISI 316L, formation of higher percentage of δ ferrite in interdendritic region has deleterious effect on mechanical properties and corrosion resistance of the joint. The scale of solidification structure is dominated by the cooling rate; higher cooling rate will produce finer dendrites, whereas lower value will produce coarse dendrites. In Fig. 20.6, higher magnification SEM micro-structure of weld interior for both the welding conditions is shown. Higher cooling rate of S1 weld condition (333 K/s) leads to fine micro-structure as compared to S2 weld condition (308 K/s). Coarse columnar dendrites were observed in the weld interior for S2 welding condition, whereas fine interconnected equiaxed type of micro-structure was observed in S1 welding condition.
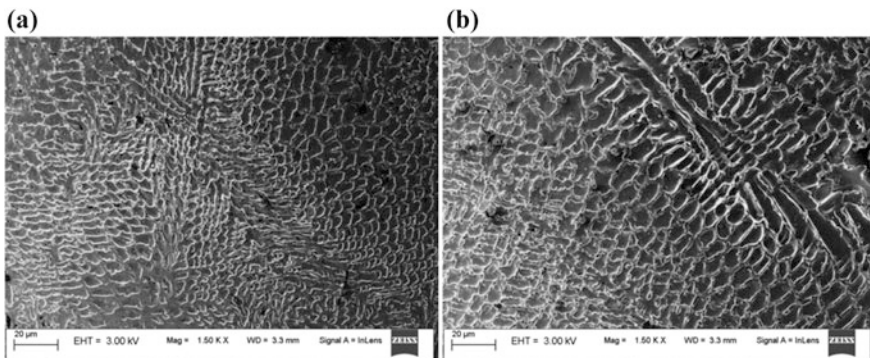

Fig. 20.6 Fusion zone micro-structure of **a** S1 and **b** S2 welding condition

Table 20.4 Results of tensile test

	Inconel 718 (base material)	AISI 316L (base material)	S1 (weld joint)	S2 (weld joint)
YS (MPa)	594	408	389	337
UTS (MPa)	878	679	653	596
Elongation (%)	23	39	26	21

The weld cooling rate plays a crucial role in controlling interdendritic segregation and formation of various intermetallic phases in the fusion zone. Lower heat input assures a higher cooling rate during the solidification that hinders the segregational tendency of solutes in the interdendritic regions, resulting in a fined micro-structure in the fusion zone. Formation of various intermetallic phases consumes a notable amount of beneficial alloying elements from the base material which results deterioration of weld quality. Hence, control of intermetallic Laves and δ-ferrite phases in the solidified zones improves mechanical properties of the joint. The tensile properties of both base and welded materials are given in Table 20.4. S1 welded samples were failed in the AISI 316L base material sides, whereas S2 welded samples were failed in the fusion zone as shown in Fig. 20.7. The tensile strength of S1 weld metal were found superior to the S2 weld material which is mainly due to the fined micro-structure of the fusion zone that reduces segregation and formation of intermetallic in the grain boundary. S1 welded sample has a tensile strength of 96% to that of the AISI 316L base material and a tensile strength of 74% to that of Inconel 718. The improvement in tensile strength of S1 welded condition is mainly attributed to the fine weld micro-structure which is mainly due to the higher cooling rate achieved during the welding process.

Cross-weld micro-hardness profile of the S1 and S2 weldments are shown in Fig. 20.8. The average micro-hardness values of base material are 219 HV and 134 HV for Inconel 718 and AISI 316L, respectively. Fusion zone of S1 welding condition has an average micro-hardness value of 154 HV, whereas for S2 welding condition, it has a lower value of 148 HV. Higher hardness of S1 fusion zone is mainly due to the fine micro-structure because of higher cooling rate. The hardness is found to be less in the HAZ region as compared to the FZ and BM, which is mainly attributed to the grain coarsening from FZ towards BM.
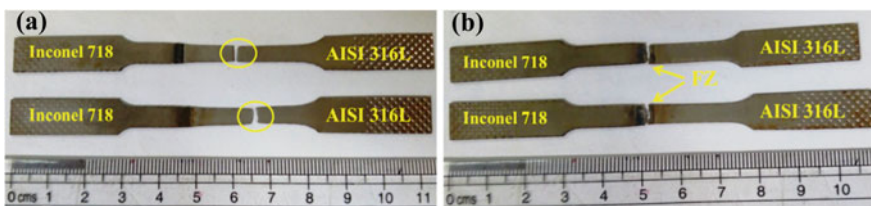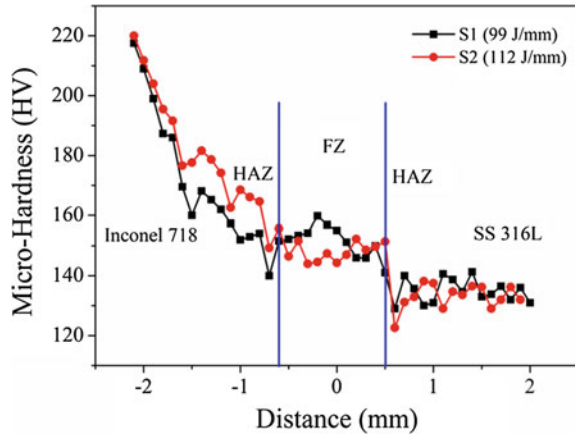

Fig. 20.7 Location of tensile fracture for **a** S1 and **b** S2 welding conditions

Fig. 20.8 Cross-weld micro-hardness distribution

20.5 Conclusion

In the present study micro-plasma arc welding between Inconel 718 with AISI 316L sheet materials with butt joint configuration has been undertaken. A three-dimensional FE-based thermal model is developed to investigate the thermal cycle during the welding process. The following conclusions were drawn from the current study

- A good agreement was obtained between the shape and size of computed and experimentally obtained weld bead.
- Full weld penetration for the bimetallic combination was achieved at a heat input of 99 J/mm.
- A maximum cooling rate of 333 K/s was calculated from the numerical model for the low heat input of 99 J/mm.
- Refinement in weld micro-structure is observed at 333 K/s cooling rate as compared to 308 K/s which results in improved joint efficiency (96.17% of AISI 316L base material) and ductility (26%) of the welded joint.
- A maximum micro-hardness difference of 6 HV is reported between the FZ of 99 and 112 J/mm welding condition.

References

1. Lee, H.T., Jeng, S.L., Yen, C.H., Kuo, T.Y.: Dissimilar welding of nickel-based Alloy 690 to SUS 304L with Ti addition. J. Nucl. Mater. **335**, 59–69 (2004)
2. Ye, X., Hua, X., Wang, M., Lou, S.: Controlling hot cracking in Ni-based Inconel-718 superalloy cast sheets during tungsten inert gas welding. J. Mater. Process. Technol. **222**, 381–390 (2015)
3. Huang, C.A., Wang, T.H., Lee, C.H., Han, W.C.: A study of the heat-affected zone (HAZ) of an Inconel 718 sheet welded with electron-beam welding (EBW). Mater. Sci. Eng., A **398**, 275–281 (2005)
4. Kumar, K.G., Ramkumar, K.D., Arivazhagan, N.: Characterization of metallurgical and mechanical properties on the multi-pass welding of Inconel 625 and AISI 316L. J. Mech. Sci. Technol. **29**, 1039–1047 (2015)
5. Henderson, M.B., Arrell, D., Larsson, R., Heobel, M., Marchant, G.: Nickel based superalloy welding practices for industrial gas turbine applications. Sci. Technol. Weld. Joining **9**, 13–21 (2004)
6. Radhakrishnan, B., Thompson, R.G.: A model for the formation and solidification of grain boundary liquid in the heat-affected zone (HAZ) of welds. Metall. Mater. Trans. A **23**, 1783–1799 (1992)
7. Janaki Ram, G.D., Venugopal Reddy, A., Prasad Rao, K., Reddy, G.M., Sarin Sundar, J.K.: Microstructure and tensile properties of Inconel 718 pulsed Nd-YAG laser welds. J. Mater. Process. Technol. **167**, 73–82 (2005)
8. Kar, J., Roy, S.K., Roy, G.G.: Effect of beam oscillation on microstructure and mechanical properties of AISI 316L electron beam welds. Metall. Mater. Trans. A **48**, 1759–1770 (2017)
9. Radhakrishna, C.H., Rao, K.P.: The formation and control of Laves phase in superalloy 718 welds. J. Mater. Sci. **32**, 1977–1984 (1997)
10. Thavamani, R., Balusamy, V., Nampoothiri, J., Subramanian, R., Ravi, K.R.: Mitigation of hot cracking in Inconel 718 superalloy by ultrasonic vibration during gas tungsten arc welding. J. Alloy. Compd. **740**, 870–878 (2018)
11. Bansal, A., Sharma, A.K., Das, S., Kumar, P.: On microstructure and strength properties of microwave welded Inconel 718/stainless steel (SS-316L). Proc. Inst. Mech. Eng., Part L: J. Mater. Des. Appl. **230**, 939–948 (2016)
12. Ramkumar, T., Selvakumar, M., Narayanasamy, P., Begam, A.A., Mathavan, P., Raj, A.A.: Studies on the structural property, mechanical relationships and corrosion behaviour of Inconel 718 and SS 316L dissimilar joints by TIG welding without using activated flux. J. Manuf. Process. **30**, 290–298 (2017)
13. Ramkumar, K.D., Patel, S.D., Praveen, S.S., Choudhury, D.J., Prabaharan, P., Arivazhagan, N., Xavior, M.A.: Influence of filler metals and welding techniques on the structure–property relationships of Inconel 718 and AISI 316L dissimilar weldments. Mater. Des. (1980–2015) **62**, 175–188 (2014)
14. Manikandan, S.G.K., Sivakumar, D., Rao, K.P., Kamaraj, M.: Effect of weld cooling rate on Laves phase formation in Inconel 718 fusion zone. J. Mater. Process. Technol. **214**, 358–364 (2014)
15. Kou, S.: Welding Metallurgy. Wiley, New Jersey, USA (2003)
16. Goldak, J., Chakravarti, A., Bibby, M.: A new finite element model for welding heat sources. MTB **15**, 299–305 (1984)
17. Rahman Chukkan, J., Vasudevan, M., Muthukumaran, S., Ravi Kumar, R., Chandrasekhar, N.: Simulation of laser butt welding of AISI 316L stainless steel sheet using various heat sources and experimental validation. J. Mater. Process. Technol. **219**, 48–59 (2015)
18. Dye, D., Hunziker, O., Roberts, S.M., Reed, R.C.: Modeling of the mechanical effects induced by the tungsten inert-gas welding of the IN718 superalloy. Metall. Mater. Trans. A **32**, 1713–1725 (2001)

19. Baruah, M., Bag, S.: Influence of heat input in microwelding of titanium alloy by micro plasma arc. J. Mater. Process. Technol. **231**, 100–112 (2016)
20. Yadaiah, N., Bag, S.: Effect of heat source parameters in thermal and mechanical analysis of linear GTA welding process. ISIJ Int. **52**, 2069–2075 (2012)
21. Aktaş Çelik, G., Polat, Ş., Atapek, Ş.H., Haidemenopoulos, G.N.: Microstructural and mechanical characterization of solidified austenitic stainless steels. Arch. Foundry Eng. **17**, 163–167 (2017)